General Disclaimer

One or more of the Following Statements may affect this Document

- This document has been reproduced from the best copy furnished by the organizational source. It is being released in the interest of making available as much information as possible.

- This document may contain data, which exceeds the sheet parameters. It was furnished in this condition by the organizational source and is the best copy available.

- This document may contain tone-on-tone or color graphs, charts and/or pictures, which have been reproduced in black and white.

- This document is paginated as submitted by the original source.

- Portions of this document are not fully legible due to the historical nature of some of the material. However, it is the best reproduction available from the original submission.

NASA TECHNICAL MEMORANDUM

NASA TM X-62,513

NASA TM X-62,513

VISCOUS/POTENTIAL FLOW ABOUT MULTI-ELEMENT TWO-DIMENSIONAL AND INFINITE-SPAN SWEPT WINGS: THEORY AND EXPERIMENT

L. E. Olson
Ames Research Center
and
U. S. Army Air Mobility R&D Laboratory
Moffett Field, California 94035

F. A. Dvorak
Analytic Methods
Bellevue, Washington

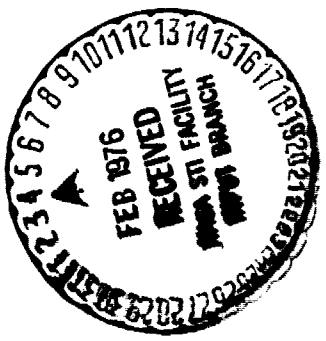

December 1975

NASA TECHNICAL MEMORANDUM

NASA TM X-62,513

NASA TM X-62,513

VISCOUS/POTENTIAL FLOW ABOUT MULTI-ELEMENT TWO-DIMENSIONAL AND INFINITE-SPAN SWEPT WINGS: THEORY AND EXPERIMENT

L. E. Olson
Ames Research Center
and
U. S. Army Air Mobility R&D Laboratory
Moffett Field, California 94035

F. A. Dvorak
Analytic Methods
Bellevue, Washington

December 1975

1. Report No.	2. Government Accession No.	3. Recipient's Catalog No.
TM X-62,513		

4. Title and Subtitle	5. Report Date
VISCOUS/POTENTIAL FLOW ABOUT MULTI-ELEMENT TWO-DIMENSIONAL AND INFINITE-SPAN SWEPT WINGS: THEORY AND EXPERIMENT	6. Performing Organization Code

7. Author(s)	8. Performing Organization Report No.
L. E. Olson and F. A. Dvorak	A-6389
	10. Work Unit No. 505-06-31
9. Performing Organization Name and Address	11. Contract or Grant No.
Ames Research Center and U.S. Army Air Mobility R&D Laboratory, Moffett Field, Calif. and Analytic Methods, Bellevue, Washington.	13. Type of Report and Period Covered
12. Sponsoring Agency Name and Address	Technical Memorandum
	14. Sponsoring Agency Code

15. Supplementary Notes

16. Abstract

The viscous subsonic flow past two-dimensional and infinite-span swept multi-component airfoils is studied theoretically and experimentally. The computerized analysis is based on iteratively coupled boundary-layer and potential flow analysis. The method, which is restricted to flows with only slight separation, gives surface pressure distribution, chordwise and spanwise boundary-layer characteristics, lift, drag, and pitching moment for airfoil configurations with up to four elements. Merging confluent boundary layers are treated. Theoretical predictions are compared with an exact theoretical potential flow solution and with experimental measures made in the Ames 40- by 80-Foot Wind Tunnel for both two-dimensional and infinite-span swept wing configurations. Section lift characteristics are accurately predicted for zero and moderate sweep angles where flow separation effects are negligible.

17. Key Words (Suggested by Author(s))	18. Distribution Statement
Aerodynamics, Airfoils, Boundary Layers, High Lift, Potential Flow, Slats, Wings, Flaps, Swept Wings, Viscous Interaction, Viscous Flows	Unlimited STAR Category 02

19. Security Classif. (of this report)	20. Security Classif. (of this page)	21. No. of Pages	22. Price*
Unclassified	Unclassified	10	$3.25

*For sale by the National Technical Information Service, Springfield, Virginia 22161

VISCOUS/POTENTIAL FLOW ABOUT MULTI-ELEMENT TWO-DIMENSIONAL AND INFINITE-SPAN SWEPT WINGS: THEORY AND EXPERIMENT

L. E. Olson*
Ames Research Center, NASA, and U.S. Army Air Mobility R&D Laboratory
Moffett Field, California
and
F. A. Dvorak†
Analytic Methods, Bellevue, Washington

Abstract

The viscous subsonic flow past two-dimensional and infinite-span swept multi-component airfoils is studied theoretically and experimentally. The computerized analysis is based on iteratively coupled boundary-layer and potential-flow analysis. The method, which is restricted to flows with only slight separation, gives surface pressure distribution, chordwise and spanwise boundary-layer characteristics, lift, drag, and pitching moment for airfoil configurations with up to four elements. Merging confluent boundary layers are treated. Theoretical predictions are compared with an exact theoretical potential flow solution and with experimental measures made in the Ames 40- by 80-Foot Wind Tunnel for both two-dimensional and infinite-span swept wing configurations. Section lift characteristics are accurately predicted for zero and moderate sweep angles where flow separation effects are negligible.

Notation

A = aerodynamic influence coefficient matrix
a = aerodynamic influence coefficient
b = wing span, m
C_d = section drag coefficient = section drag/$(\frac{1}{2}\rho_\infty U_\infty^2 C_o)$
C_{d_i} = wing induced drag coefficient = wing drag/$(\frac{1}{2}\rho_\infty U_\infty^2 C_o b)$
C_f = local skin friction coefficient
C_L = wing lift coefficient = wing lift/$(\frac{1}{2}\rho_\infty U_\infty^2 C_o b)$
C_ℓ = section lift coefficient on wing centerline = section lift/$(\frac{1}{2}\rho_\infty U_\infty^2 \cos^2\beta C_o)$
C_o = reference chord, m
C_p = pressure coefficient = $(p - p_\infty)/(\frac{1}{2}\rho_\infty U_\infty^2 \cos^2\beta)$
D = minimum distance between adjacent elements
H = shape factor = δ^*/θ
$\vec{n}_k$ = component of freestream velocity normal to panels of kth component
p = static pressure, $kNnm^{-2}$
q = source strength
r = viscous/potential flow iteration relaxation factor
R = Gauss-Seidel relaxation factor
Re = Reynolds number = $U_\infty C_o/\nu$
$R\theta$ = Reynolds number based on momentum thickness = $U_e\theta/\nu$
s = boundary-layer coordinate along surface in chordwise direction, m
u = chordwise velocity, ms^{-1}
v = spanwise velocity, ms^{-1}
x,y = chordwise and spanwise wing coordinates, m
z = boundary-layer coordinate normal to airfoil surface, m
α = angle of attack
β = sweep angle
γ = vorticity
δ = panel angle relative to reference coordinate system
δ^* = chordwise displacement thickness, m
θ = momentum thickness, m
ν = kinematic viscosity, m^2s^{-1}

Subscripts

e = edge of viscous layer
exp = experimental value
f = flap
i,j = panel indices
k = component indice
te = trailing edge
vlt = vortex-lattice theory
w = wing
ℓ = wing centerline
∞ = freestream value

Superscripts

I = index of viscous/potential flow iteration
ν = index of Jacobi and Gauss-Seidel iteration

I. Introduction

The multi-component wing is an essential element of the high-lift system of nearly all general aviation, commercial, and military aircraft. Due to the high-lift requirement, the influence of viscosity becomes a dominant factor in determining aerodynamic performance. As a result, inviscid theory is not sufficient and viscous effects must be considered if accurate predictions are to be made.

Design of these systems has generally been dependent on experimental verification of predicted aerodynamic performance. A prime example is configuration optimization where optimum slat and flap positions and deflections for best aerodynamic performance are generally determined through expensive and time consuming wind tunnel testing. Improved understanding of the aerodynamic phenomena and improved predictive capability would significantly reduce this wind tunnel effort and permit optimization in the early design stages.

Stevens, Goradia, and Branden[1] present a theoretical analysis for two-dimensional flow about multi-component airfoils where for the first time the merging of a wing wake and the upper-surface boundary layer of a downstream element is treated analytically for configurations with up to four elements. Bhateley and McWhirter[2] and Callaghan and Beatty[3] also present analyses for two-dimensional multi-component configurations although neither of these papers treats wake-boundary layer merging effects. The work of Jacob and Steinbach[4] considers multi-element airfoils with flow separation and Ormsbee and Chen[5] present a method for designing multi-component airfoils for maximum lift.

*Aerospace Engineer, Member AIAA
†President

The objective of the present work is to begin the extension of multi-component airfoil analysis into three-dimensional flows by considering the subsonic flow about swept wings of infinite aspect ratio. The basic analytic method is outlined in Section II. The present analysis extends the theoretical method of Dvorak and Woodward[6] and compares predicted results with experiment. The theoretical extension of the work of Ref. 6 includes: 1) introduction of advanced potential-flow solution techniques; 2) modification of the viscous/potential flow coupling when only slight separation is present; and, 3) use of under-relaxation of surface source distributions in the iterative coupling of the viscous and potential flow solutions. In the supporting experimental program, tests of a two-element configuration were conducted in the Ames 40- by 80-Foot Wind Tunnel. The basic objective of this testing was to obtain experimental data on two-dimensional and infinite aspect ratio swept-wing configurations. The experimental program is described in Section III and the results are compared with the theoretical predictions in Section IV.

II. Theoretical Method

General

The basic theoretical method is to couple iteratively potential-flow and boundary-layer analysis. The analysis is limited to flows with negligible upper-surface separation on any element. Provided there is no strong viscous interaction, limited lower surface separation closed bubbles, such as often occur in the cove on the lower surface of a wing with a slotted flap, are permitted. In the case of the infinite-span swept wing it is assumed that all spanwise gradients in the potential and viscous flows are equal to zero. Thus, in planes normal to the leading edge, the potential flow equations reduce to the two-dimensional form. For the infinite-span swept wing the chordwise boundary-layer characteristics are of primary interest. For the laminar case Jones[7] shows that the chordwise boundary layer is essentially independent of the spanwise boundary layer. For the turbulent case this uncoupling is not possible and the spanwise and chordwise boundary-layer equations must be solved simultaneously.

Geometry Definition

Up to four elements can be analyzed, with each element represented by as many as 60 pairs of surface coordinates. Each individual slat or flap segment location is related to the main wing or reference coordinate system by pivot point coordinates prescribed in both the main element coordinate system and the individual slat or flap segment coordinate system. The selection of a rotation angle measured relative to the main component completes the specification of the element position. It is generally convenient to pivot a leading-edge device about its trailing edge and to pivot a flap about its leading edge although the hinge point of a flap could, for example, provide a ready reference point. Also, as part of the geometry definition, the flap upper-surface longitudinal radius of curvature is determined using cubic splines for later use in the finite-difference boundary-layer calculations.

Potential Flow Analysis

The potential flow analysis is performed in a plane normal to the wing leading edge. The analysis is a method of singularities where each element is represented by a closed polygon of planer panels connecting the input coordinate pairs. A linear vorticity distribution is located along each panel with the requirement that the vorticity distribution be continuous across the panel corner points. Thus, if there are n panels there are n + 1 unknowns to be determined. The boundary condition of no flow through the surface, applied at each of the panel centers, provides n equations. The additional equation required to close the system is supplied by specifying that the upper- and lower-surface velocities have a common limit at the trailing edge (i.e., the Kutta condition). This implies that the upper- and lower-surface vorticities be equal and opposite. For a unit freestream velocity the resulting system of equations to be solved for an airfoil with n panels is then

$$\begin{bmatrix} a_{11} & a_{12} & \cdots & a_{1n} \\ a_{21} & a_{22} & & \\ \cdot & & \cdot & \\ \cdot & & & \cdot \\ a_{n1} & & & a_{nn} \end{bmatrix} \begin{bmatrix} \gamma_1 \\ \gamma_2 \\ \cdot \\ \cdot \\ \gamma_n \end{bmatrix} = \begin{bmatrix} \sin(\alpha - \delta_1) \\ \sin(\alpha - \delta_2) \\ \cdot \\ \cdot \\ \sin(\alpha - \delta_n) \end{bmatrix} \tag{1}$$

or in vector form

$$[A][\vec{\gamma}] = [\vec{n}] \tag{2}$$

where the nth column represents the combined influence coefficients for the upper- and lower-surface trailing edge vorticity panels.

If the trailing edge closes the vorticity must go to zero because the trailing edge then becomes a stagnation point. Although this solution is automatically given by Eq. (1) the geometry is often such that the influence coefficients in the nth column are quite small with the result that the matrix is poorly conditioned. In this case an alternate Kutta condition is used which specifies that the upper and lower trailing-edge vorticity strengths are equal to zero at the trailing edge. An additional unknown is supplied by introducing a constant strength source distribution on the surface of the airfoil. The resulting system of equations is the same as Eq. (1) except for the nth column of vorticity influence coefficients. That column is replaced by the constant source-distribution influence coefficients and γ_n is the unknown source distribution strength.

For a multi-element configuration with j components Eq. (2) can be written

$$\begin{bmatrix} A_{11} & A_{12} & \cdots & A_{1j} \\ A_{21} & A_{22} & & \\ \cdot & & \cdot & \\ \cdot & & & \cdot \\ A_{n_2} & & & A_{ji} \end{bmatrix} \begin{bmatrix} \vec{\gamma}_1 \\ \vec{\gamma}_2 \\ \cdot \\ \cdot \\ \vec{\gamma}_j \end{bmatrix} = \begin{bmatrix} \vec{n}_1 \\ \vec{n}_2 \\ \cdot \\ \cdot \\ \vec{n}_j \end{bmatrix} \tag{3}$$

$$A_{ij} = \begin{cases} i = j & \text{self-influence coefficient matrix of component } i \\ i \neq j & \text{influence coefficient matrix of } j\text{th component on the } i\text{th component} \end{cases}$$

$\vec{\gamma}_k$ = vorticity strength vector for kth component

Equation (3) is solved by direct triangular decomposition (see, for example, Isaacson and Keller[8]) for single component airfoils. At the users option, triangular decomposition can also be used on multi-component configurations with a total of less than 100 panels. For multi-component configurations two iterative methods were investigated: block-Jacobi iteration, and block-Gauss-Seidel iteration with relaxation. The solution is found by starting with some assumed initial solution vector,

$$\begin{bmatrix} \vec{\gamma}_1 \\ \vec{\gamma}_2 \\ \cdot \\ \cdot \\ \cdot \\ \vec{\gamma}_j \end{bmatrix}^{(0)} \tag{4}$$

The νth iteration is then expressed in one of the following ways:

1. Block Jacobi iteration:

$$\vec{\gamma}_k^{(\nu)} = A_{kk}^{-1}\left[\vec{n}_k - \sum_{\ell=1}^{j} A_{\ell k}\vec{\gamma}_\ell^{(\nu-1)}\right] \quad \begin{matrix} k = 1,2,\ldots,j \\ \nu = 1,2,\ldots \end{matrix} \tag{5}$$

2. Block-Gauss-Seidel iteration with relaxation:

$$\overline{\vec{\gamma}_k^{(\nu)}} = A_{kk}^{-1}\left[\vec{n}_k - \sum_{\ell=1}^{k-1} A_{\ell k}\vec{\gamma}_\ell^{(\nu)} - \sum_{\ell=k+1}^{j} A_{\ell k}\vec{\gamma}^{(\nu-1)}\right]$$

$$\vec{\gamma}_k^{(\nu)} = R\overline{\vec{\gamma}_k^{(\nu)}} + (1 - R)\,\vec{\gamma}_k^{(\nu-1)} \quad \begin{matrix} k = 1,2,\ldots,j \\ \nu = 1,2,\ldots \end{matrix} \tag{6}$$

Equations (5) and (6) are solved using triangular decomposition on the first iteration; the decomposed matrices are saved for use on subsequent iterations. The iteration process is assumed to be converged when

$$\underset{i=1\to n}{\text{Max}}\left|\gamma_i^{\nu} - \gamma_i^{\nu-1}\right| < \varepsilon$$

where ε is generally taken to be 0.01.

For configurations with two or three lifting elements, the Gauss-Seidel without relaxation (R=1) converges in approximately one-half the number of iterations required for the Jacobi method. Since the number of arithmetic operations per iteration are nearly equal for the two methods, the Gauss-Seidel method was selected as the best iterative technique.

As one might expect the optimum relaxation factor for the Gauss-Seidel method is dependent on how closely the various lifting elements are coupled. For example, consider an airfoil with a single slotted flap. If the flap is moved off to infinity the two elements are essentially uncoupled. The off-diagonal block matrices of Eq. (3), which model the component interactions, are zero and two iterations of Eq. (6) give convergence (first iteration gets the solution and the second is required only to check the first). As $|R-1|$ increases, the number of iterations required also increases.

If the elements are located in close proximity, as is typically the case, the interaction between components become important. Again, consider the single slotted flap. Assuming the initial solution ($\vec{\gamma}_k^{(0)}$, k = 1,2) is a null vector, the final coupled solution is obtained from Eq. (6) for R=1 as follows: 1) $\vec{\gamma}_1^{(1)}$ is the solution vector for the main component in free air (because the upwash field from the flap is not present, the lift level for this component will be less than that for the coupled system); 2) $\vec{\gamma}_2^{(1)}$ is the solution for the flap in the downwash field of a wing that is carrying reduced lift, relative to the coupled system (this reduced downwash field causes the flap to carry excess lift); and 3) on the next iteration the wind lift will be too high because of the excess upwash from the flap. Similarly the flap lift on the second iteration will be below that for the correctly coupled system.

This oscillatory behavior indicates that under-relaxation should accelerate the rate of convergence and the amount of under-relaxation required should increase as the elements are moved closer together. An "optimum" relaxation factor given by $R = 1 - \exp -10 \underset{i=1\to k-1}{\text{Min}}(D_i)$ was determined by numerical experiments with two and three element configurations. D_i is the minimum distance in fraction of chord between the trailing edge of the ith component and the upper surface of the following component. With this relaxation factor the number of iterations required for convergence was generally reduced by a factor of 3 below that required with R = 1.

Computational times required for the direct method of solution have been compared to the computational times required for block-Gauss-Siedel iteration with relaxation method. The test cases were closely coupled two-component configurations. The total number of panels used for these comparisons was approximately 100. The iterative method obtained the converged solution in approximately one-half the time required by the direct method. Increasing the number of elements, and thus the total number of equations to be solved, had no significant impact on the number of iterations required by the iterative method. Thus the advantage of the iterative method over the direct will increase as the number of elements is increased.

The pressure coefficient at the center of each panel is calculated from the surface velocity at that point. The lift and pitching-moment coefficients are obtained by integrating the pressures around the airfoil.

A comparison of the present method with the exact conformal mapping solution of Williams[9] for

a two element case is shown in Fig. 1. The angle of incidence is 0° and the flap deflection is 30°; agreement with the exact solution is excellent.

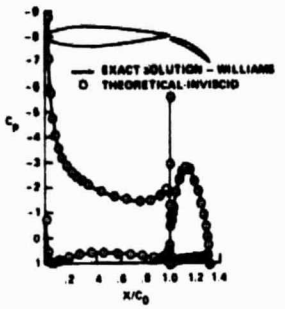

Fig. 1 Comparison of numerical and exact potential flow solutions: $\alpha=0°$, $\delta_f=30°$.

Boundary-Layer Analysis

As outlined in Fig. 2, a combination of integral and finite difference techniques are used. Integral methods are used for conventional boundary layers because of their computational efficiency whereas a finite-difference method is used for the more complex confluent boundary-layer analysis. The stagnation line, conventional boundary-layer, and confluent boundary-layer methods are discussed in the following sections.

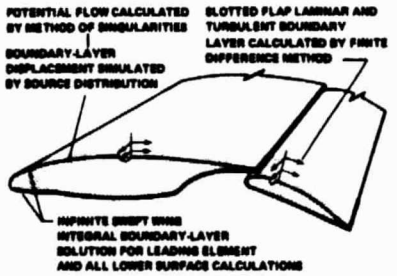

Fig. 2 Flow about swept, infinite-span, multi-element wing.

Stagnation Line Flow

Cumpsty and Head[10] experimentally investigated the stagnation-line flow characteristics of infinite-span swept wings. They found that the stagnation line boundary-layer integral parameters (H, θ, and C_f) and the state (laminar or turbulent) correlate with the parameter $C^* = v_e^2/(\nu\frac{du_e}{ds})$. The stagnation line boundary-layer characteristics on each element are determined using these correlations.

Conventional Boundary-Layer Methods

Integral boundary-layer methods are used for all conventional boundary layers, such as the upper- and lower-surface boundary layers of all elements, and the upper-surface boundary layers of following elements up to the slot exists.

The two-dimensional equations of Curle[11] are solved along external streamlines to determine the laminar boundary-layer characteristic. It is assumed that laminar cross-flow effects have a negligible influence on the overall calculation, at least for moderate sweep angles. Once the boundary-layer characteristic along the potential flow streamlines have been determined, the spanwise and chordwise parameters are determined.

These chordwise boundary-layer characteristics are used with the correlations of Smith[12] to determine the point of laminar instability. These correlations relate R_θ to a pressure gradient parameter. Knowing the point of instability, R_θ, and the pressure gradient; the location at which full transition has occurred is determined by using the correlations of Granville.[13] The integral method of Cumsty and Head[14] for boundary layers on infinite-span swept wings is used for the turbulent calculation.

Should laminar separation occur prior to transition, the correlations of Gaster[15] are used to determine whether turbulent reattachment occurs. If reattachment is predicted, the calculation continues as a turbulent flow; if catastrophic separation is predicted, the calculation is terminated.

Confluent Boundary-Layer Method

The finite-difference method used to solve the infinite-span swept-wing, confluent boundary-layer equations is described by Crank and Nicholson[16] and by Dvorak and Head.[17] The eddy viscosity model used here is a modification of the two-dimensional method for wall jets and turbulent boundary-layers developed by Dvorak.[18] These calculations include the effects of longitudinal surface curvature. The static pressure field, p(s,z), which is required for the solution of the boundary-layer equations, is determined directly from the potential flow solution.

The initial conditions required to start the finite-difference calculation at the slot exit are constructed from: 1) the integral boundary-layer solution at the slot exit on the upper surface of the component in question; 2) the laminar potential core as determined from the potential-flow solution; and 3) the upper- and lower-surface boundary-layer solutions at the trailing edge of the upstream element. If cove separation is present the boundary layer at the slot exit from the lower surface of the upstream element is assumed to follow the one-seventh power law with a thickness equal to one-third the slot-exit width. This assumed profile is representative of what is observed experimentally. With these initial conditions and with the static pressure field known, the boundary-layer equations are solved in a forward marching fashion to the trailing edge of the component.

The profile drag for a streamwise section is determined by use of the method of Squire and Young[19]:

$$C_d = 2\left(\frac{\theta}{C}\right)_{te}\left(\frac{u_e}{u_\infty}\right)_{te}^{\frac{H_{te}+5}{2}} \qquad (7)$$

III. Viscous/Inviscid Coupling

The effect of boundary-layer displacement and mass entrainment on the potential flow is simulated by distributed sources on the panels used to describe the airfoil contour. The strengths of these source panels as determined directly from the boundary-layer solutions are $q = \frac{d}{ds}(u_e\delta^*)$ where

u_e is the chordwise potential-flow velocity at the edge of the boundary layer and δ^* is the boundary-layer displacement thickness given by

$$\delta^* = \int_0^{z_e} (1 - \frac{u}{u_e})dz \qquad (8)$$

A modified Kutta condition, which requires that the flow be tangential to the trailing edge panel at the trailing edge on the upper and lower surfaces, together with the boundary condition that the velocity normal to the surface be equal to the known source distribution, determines the potential flow. The resulting potential-flow pressure distribution is then used in subsequent boundary-layer calculations.

It has been observed (e.g., Brune, Rubbert, and Nark[20]) that conventional cyclic boundary-layer/inviscid flow matching usually results in a divergent or, at best, a slowly convergent iteration process, especially if the viscous interaction is relatively strong (as is often the case for high-lift configurations). In the present method the boundary-layer source distribution is under-relaxed according to the formula

$$q^{I+1} = q^I + r(\overline{q^I} + q^I) \qquad (9)$$

where q^I is the source distribution strength used in the ith potential flow solution and $\overline{q^I}$ is equal to $\frac{d}{ds}(u_e\delta^*)$ obtained from the ith boundary-layer solution. A relaxation factor of 0.5 has been found to be sufficient for a large variety of configurations.

For the unswept case, separation is defined as the location where the skin friction goes to zero. For the swept case, separation is defined as the point where the wall skin-friction vector forms a 90° angle with the local potential-flow velocity vector. The manner in which the viscous interaction is handled depends on what type of separation is being considered. If separation occurs at some point, $\left(\frac{s}{c_o}\right)_{sep}$, on the upper surface of a component, the boundary layer calculation is necessarily terminated at that point. Based on the experimental observation that the static pressure is nearly constant in the separated flow, u_e is assumed constant and equal to its value at the separation point.

The displacement thickness in the separated zone is obtained by linear extrapolation from the point of separation. Thus, in the separated zone the blown boundary condition becomes $q = \left(u_e \frac{d\delta^*}{ds}\right)_{sep}$. The method is not intended to model extensive flow separation; rather, the intent is to permit the calculation to continue if separation occurs, such as is often encountered after the first potential flow solution. Separation on the lower surface of the last element, which seldom occurs, is handled similarly. Lower-surface flow separation, such as might be encountered in a flap cove, is handled differently. Experimental observation indicates that even if cove separation occurs the boundary layer at the slot exit is generally thin and its displacement effect on the potential flow is expected to be minimal. Therefore, the source distribution in the cove-separation zone is assumed to be a linear interpolation made between its value at separation and zero at the trailing edge.

IV. Wind Tunnel Test Program

Model

The rectangular planform finite wing, used in the experimental part of this study, is shown as it was mounted in the Ames 40- by 80-Foot Wind Tunnel in Fig. 3. This wing is equipped with a full-span, 40% chord, single slotted flap. The wing and flap were basically steel frameworks covered with wood; the wood in turn was coated with a glass reinforced plastic skin to give the desired contour. The wing span was 16 m with a reference chord of 1.7 m and a nominal extended chord of 2.1 m. The relatively high aspect ratio of 7.6 (based on the extended chord), combined with the uniform section is designed to provide a nearly constant span loading over the wing center section. In addition, the finite wing avoids the interference effects, caused by wind-tunnel side-wall junctions, that are usually encountered with models that span the test section. These interference effects become especially troublesome at high lift and when separation plays a significant role.

Fig. 3 Model mounted in 40- by 80-Foot Wind Tunnel

The flap brackets, which remain parallel to the chordwise direction when the wing is yawed, permit horizontal and vertical flap movement. The range of movement in the chordwise and normal-to-chord direction was 5% and 4% of C_o respectively.

The basic airfoil section from which the wing-flap combinations were derived is an RAE 2815. The wing-flap combinations tested are shown in Fig. 4. A complete table of coordinates is listed by Foster et al.[21] The 10° flap configuration had a faired cove whereas the 30° flap configuration had no cove fairing; the leading edge of the 30° flap configuration was drooped 10° with the pivot point

on the lower surface at an x_w/C_0 of 0.15. The test Reynolds number, R_e, was 3.8×10^6.

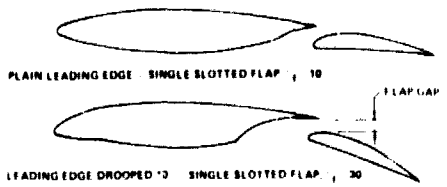

Fig. 4 Airfoil configurations tested.

Wing Forces and Moments

Overall wing forces and moments were obtained from the wind tunnel scale system and corrected for tunnel wall-interference effects. The total lift was used in conjunction with the vortex lattice theory of Hough[22] to determine a section angle of attack at the center section of the wing according to the formula

$$\alpha = \alpha_w - \Delta\alpha_i \qquad (10)$$

where $\Delta\alpha_i$ is the induced angle of attack at the center section due to finite wing effects. The induced angle of attack, or mean downwash at the wing center line, as given by the vortex lattice theory is

$$\Delta\alpha_i = \left[\frac{1}{C_L}\left(\frac{C_{d_i}}{C_\ell}\right)_{\bar{q}}\right]_{vlt}(C_L)_{exp} \qquad (11)$$

where it is assumed that the induced angle of attack scales with the measured total lift of the wing.

Pressure Measurement:

The center section of the wing was instrumented with three chordwise rows of static pressure orifices. One row was located on the model centerline, a second row at $y = 0.44\ C_0$, and a third row at $y = -0.22\ C_0$. No flap brackets were located between $y = -0.22\ C_0$ and $y = 0.44\ C_0$. At each of these three spanwise stations there were 64 orifices on the main element and 30 orifices on the flap. The method of measuring pressures was with scanivalves and transducers with ranges of ±17kN m^{-2}(±2.5lb/in^2); the scanivalves were automatically sequenced. The transducer output was digitized and punched onto data cards for subsequent data reduction on a digital computer.

Preliminary tests at sweep angles of 0° and 25° showed no significant spanwise gradients in the center section of the wing. All data presented in this paper were obtained on the model centerline.

Hot-Wire Boundary-Layer Surveys

Velocity profiles near the main element trailing edge and above the flap upper surface were obtained using a translating hot-wire probe. The drive motor was located inside the flap, thus minimizing the aerodynamic interference due to the survey device. Anemometer output was linearized to give a linear relationship between voltage and velocity and then recorded on a X-Y plotter as a function of probe position.

Hot-wire calibrations were made using a free jet powered by a variable speed blower. The anemometer bridge was temperature compensated to minimize the influence of wind-tunnel static-temperature variation on anemometer output.

V. Comparison of Theoretical and Experimental Results

Section Lift

Figures 5-7 show comparisons of the measured section lift characteristics, as functions of section angle of attack, with those determined theoretically. Figure 5 is for the 10° flap configuration without sweep; Fig. 6 is for the 30° flap configuration with 0° sweep; and Fig. 7 is for the 30° flap configuration with 25° sweep. The theoretical calculations have been terminated at the angle of attack where upper-surface separation first occurred. This type of separation greatly inhibited or prevented convergence of the viscous-potential flow iteration process, and resulted in generally unreliable results. The fact that in all cases separation occurred at lift levels below, but within 10% of, $C_{\ell_{max}}$ indicates that the existence of separation on either the main component or flap provides a reasonably accurate and conservative estimate of maximum lift.

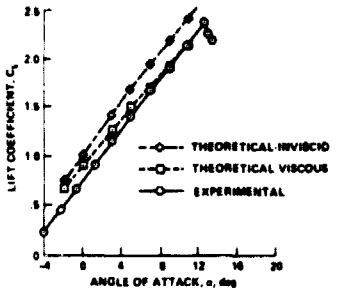

Fig. 5 Section lift characteristics for plain leading edge: $\beta = 0°$, $\delta_f = 10°$.

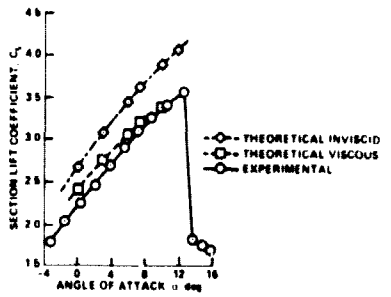

Fig. 6 Section lift characteristics for drooped leading edge: $\beta = 0°$, $\delta_f = 30°$.

The general character of the results for the three configurations shown in Figs. 5-7 are similar. Comparison of the experimental measurements and the potential-flow solutions show strong viscous interactions resulting in observed lift coefficients well below those predicted by pure potential-flow theory. The addition of viscous interaction effects brings the theoretical predictions into much better agreement with the experimental results with the largest difference occurring, somewhat surprisingly, at lower angles of attack. The reason why the lift is

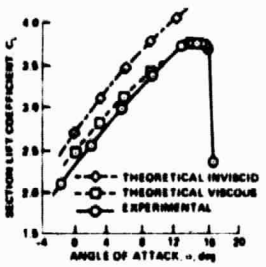

Fig. 7 Section lift characteristics for drooped leading edge: $\beta = 25°$, $\delta_f = 30°$.

over-predicted at the lower angles of attack is shown by the section pressure distributions presented in Figs. 8 and 9.

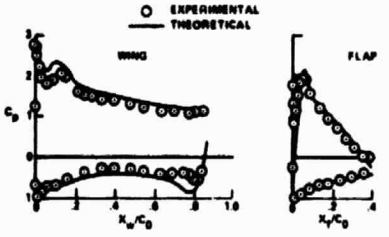

Fig. 8 Section pressure distribution for dropped leading edge: $\alpha = 0°$, $\beta = 0°$, $\delta_f = 30°$.

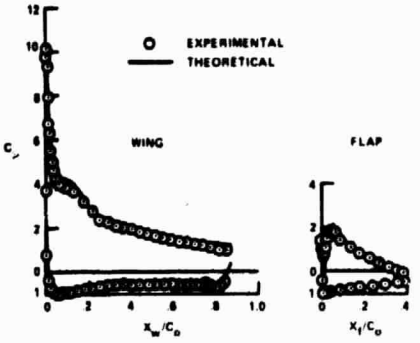

Fig. 9 Section pressure distribution for drooped leading edge: $\alpha = 7.5°$, $\beta = 0°$, $\delta_f = 30°$.

The flap pressure distribution for the unswept 30° flap configuration of Fig. 8 is predicted quite accurately, whereas the load level for the main element is over-predicted. This discrepancy is attributed to extensive flow separation in the cove on the lower surface of the main component. This separation, although predicted by the boundary-layer analysis, results in a strong viscous interaction which is not modeled accurately in the theoretical analysis.

As a result, the contribution to lift of the pressure distribution in the cove is over-predicted. In addition, the cove separation appears to have reduced the net circulation on the main element, thereby influencing the upper surface pressure distribution as well. At higher angles of attack, such as the 7.5° shown in Fig. 9, the orientation of the cove relative to the freestream is such that the influence of cove separation (although still present) is suppressed; the result is a much improved agreement between theory and experiment. Increasing the sweep angle to 25° did not significantly alter this behavior for either the 10° or 30° flap configurations.

Figure 10 compares the effect of angle of attack on computed integral boundary-layer characteristics with its effect on experimentally measured characteristics for the unswept 10° flap configuration. The comparisons are made for a point located at the trailing edge of the main component upper surface. The shape factor, $H = \frac{\delta^*}{\theta}$, is predicted accurately throughout the angle of attack range. The tendency to slightly over-predict the displacement thickness is caused, at least in part, by the increased wing loading due to the previously mentioned cove separation effects.

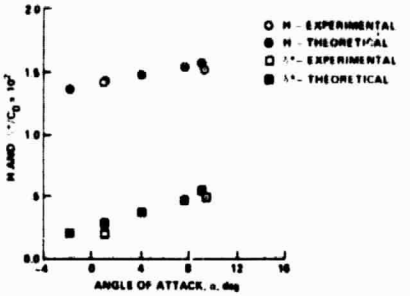

Fig. 10 Shape factor and displacement thickness at wing upper surface trailing edge: $\beta = 0°$, $\delta_f = 30°$.

Velocity profiles on the flap upper surface for the 30° flap configuration are shown in Figs. 11 and 12 for an angle of attack of 9°. The mean velocity profile in Fig. 11 is for a station 0.5% downstream of the main component trailing edge. The dominate feature is the wake from the main component. The hot-wire probe in this case did not get close enough to the flap upper surface to get into the very thin flap upper-surface boundary layer. Agreement between theory and experiment is reasonably good. Inspection of the mean velocity profile indicates, as assumed in the theoretical analysis, that a laminar core exits in the slot efflux. Also shown in Fig. 11 is the turbulence level, $\sqrt{u'^2}/u_e$, which provides a qualitative measure of the potential for turbulent transport. The turbulence level, significant throughout the slot efflux, indicates that a true laminar core is not present. This turbulence is undoubtedly comprised of remnants of the turbulent mixing process associated with the cove separation. The predicted and measured velocity profiles at the flap trailing edge are compared in Fig. 11. Although the total boundary-layer thickness and the point of minimum velocity associated with the wing wake are predicted accurately, the experimental measurements show that the wing wake and flap boundary layer have merged to a greater extent than that predicted theoretically implying that the turbulence in the so-called laminar core has a significant influence on the confluent boundary-layer development.

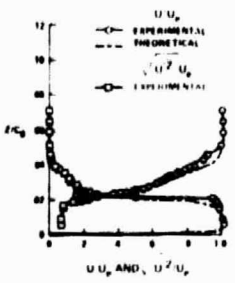

Fig. 11 Boundary-layer velocity and turbulence profiles downstream of wing trailing edge: $\alpha = 9°$, $\beta = 0°$, $\delta_f = 10°$, $x_f/C_o = 0.036$.

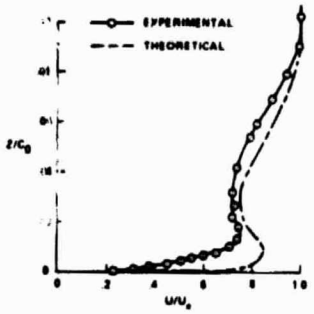

Fig. 12 Boundary-layer velocity profiles at flap trailing edge: $\alpha = 9°$, $\beta = 0°$, $\delta_f = 10°$, $x_f/C_o = 0.39$.

Figure 13 shows a comparison of the computed drag for the 30° flap configuration with the drag measurements obtained from Ref. 21 for the two-dimensional case. Although the shape of the lift-drag curve is correct, the theoretical method consistently over-predicts the drag; this suggests that the method of Squire and Young[19] is not directly applicable to multi-component airfoils.

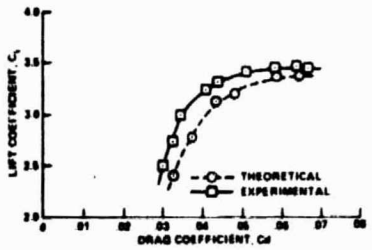

Fig. 13 Lift versus drag for drooped leading edge: $\beta = 0°$, $\delta_f = 30°$.

Figure 14 illustrates the application of the theoretical method to a configuration optimization problem. In this figure the effect of flap gap on lift at a fixed angle of attack is compared with the theoretical prediction for the 30° flap configuration. The optimum flap gap of 2% of chord is predicted quite accurately.

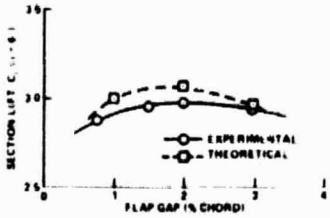

Fig. 14 Effect of flap gap on section lift for drooped leading edge: $\alpha = 6°$, $\beta = 0°$.

Concluding Remarks

A theoretical method for analyzing the viscous/potential flow around two-dimensional and infinite-span multi-component airfoils has been described. The analysis is based on iteratively coupled boundary-layer and potential-flow calculations. The viscous-flow analysis considers the confluent boundary layer, where appropriate, and computes both spanwise and chordwise boundary-layer characteristics. In support of the theoretical program an experimental study was conducted in the Ames 40- by 80-Foot Wind Tunnel. Comparisons of the present theoretical method with other exact solutions and with the experimental data resulted in the following conclusions:

1. The present theoretical method accurately predicts section lift characteristics of multi-component configurations through moderate sweep angles where flow separation effects are negligible.

2. For the configurations tested, the angle of attack for the first occurrence of upper surface separation defines a reasonably accurate and conservative estimate of $C_{\ell_{max}}$ at sweep angles of 0° and 25°.

3. The present method accurately predicts the optimum flap gap for maximum lift at a fixed angle of attack.

4. In addition to the study of two-dimensional and infinite-span swept multi-component airfoils, this method will be useful in the analysis of the high-lift characteristics of relatively high aspect ratio, moderately swept, finite wings.

5. The influence of cove separation on the state (laminar or turbulent) of the slot efflux can have a strong influence on the development of the confluent boundary layer over the flap upper surface.

6. The method of Squire and Young for computing drag does not (in its original form) accurately predict the drag of multi-component configurations.

7. Potential-flow matrix computer solution times for multi-component configurations are significantly reduced, from those required for direct triangular decomposition solution, by using block-Gauss-Siedel iteration with relaxation.

8. The present potential-flow method, which utilizes linear vorticity, gives excellent agreement with exact solutions for the inviscid flow around multi-component configurations.

References

[1]Stevens, W. A., Goradia, S. H., and Braden, J. A., "Mathematical Model for Two-Dimensional Multi-Component Airfoils in Viscous Flow," NASA CR-1843, July 1971.

[2]Bhateley, Ishwar C. and McWhirter, Jack W., "Development of Theoretical Method for Two-Dimensional Multi-Element Airfoil Analysis and Design," AFFDL-TR-72-96, Aug. 1972.

[3]Callaghan, J. G. and Beatty, T. D., "A Theoretical Method for the Analysis and Design of Multi-Element Airfoils," J. Aircraft, Vol. 9, No. 12, Dec. 1972.

[4]Jacob, K. and Steinbach, D., "A Method for Prediction of Lift for Multi-Element Airfoils with Separation," AGARD-CP-143, V/STOL Aerodynamics, April 1974.

[5]Ormsbee, Allen I. and Chen, Allen W., "Multiple Element Airfoils Optimized for Maximum Life Coefficient," AIAA J., Vol. 10, No. 12, Dec. 1972.

[6]Dvorak, F. A. and Woodward, F. A., "A Viscous/Potential Flow Interaction Analysis Method for Multi-Element Infinite Swept Wings," Vol. 1, NASA CR-2476, Nov. 1974.

[7]Jones, Robert T., "Effects of Sweepback on Boundary Layer and Separation," NACA Rep. No. 884, 1947.

[8]Isaacson, Eugene and Keller, Herbert Bishop, Analysis of Numerical Methods, John Wiley & Sons, Inc., New York, 1966.

[9]Williams, B. R., "An Exact Test Case for the Plane Potential Flow About Two Adjacent Lifting Airfoils," RAE Tech. Report 71197, Sept. 1971.

[10]Cumpsty, N. A. and Head, M. R., "The Calculation of the Three-Dimensional Turbulent Boundary Layer, Part III: Comparison of Attachment-Line Calculations with Experiment," Aeronaut. Quart., Vol. XX, May 1969.

[11]Curle, H., "A Two Parameter Method for Calculating the Two-Dimensional Incompressible Laminar Boundary Layer," J. Roy. Aeronaut. Soc., Vol. 71, 1967.

[12]Smith, A. M. O., "Transition, Pressure Gradient and Stability Theory," Proc. 9th Internat. Congress of Appl. Mech., Vol. 7, Brussels, 1957.

[13]Granville, P. S., "The Calculation of the Viscous Drag of Bodies of Revolution," David W. Taylor Model Basin Report 849, 1953.

[14]Cumpsty, N. A. and Head, M. R., "The Calculation of Three-Dimensional Turbulent Boundary Layers, Part II: Attachment-Line Flow on an Infinite Swept Wing," Aeronaut. Quart., Vol. XVIII, May 1967.

[15]Gaster, M., "The Structure and Behavior of Laminar Separation Bubbles," ARC 28-226, 1967.

[16]Crank, J. and Nicholson, P., "A Practical Method for Numerical Evaluation of Solutions of Partial Differential Equations of the Heat Conduction Type," Proc. Camb. Philos. Soc., Vol. 43, 1947.

[17]Dvorak, F. A. and Head, M. R., "Heat Transfer in the Constant Property Turbulent Boundary Layer," Brit. ARC R&M No. 1838, 1937.

[18]Dvorak, F. A., "Calculation of Turbulent Boundary Layers and Wall Jets over Curved Surfaces," AIAA J., Vol. 11, No. 4, April 1973.

[19]Squire, H. B. and Young, A. D., "The Calculation of the Profile Drag of Airfoils," Brit. ARC, R&M No. 1838, 1937.

[20]Brune, G. W., Rubbert, P. E. and Nark, T. C., "A New Approach to Inviscid Flow/Boundary Layer Matching," AIAA Paper No. 74-601, AIAA 7th Fluid and Plasma Dynamics Conference, Palo Alto, Calif., June 17-19, 1974.

[21]Foster, D. N., Irwin, H. P., and Williams, B. R., "The Two Dimensional Flow Around a Slotted Flap," RAE Tech. Report 70164, Sept. 1970.

[22]Hough, Gary R., "Remarks on Vortex Lattice Theory," J. Aircraft, Vol. 10, No. 5, May 1975.